

Large-Conductance Transmembrane Porin Made from DNA Origami

Kerstin Göpfrich,^{†,§} Chen-Yu Li,^{‡,§} Maria Ricci,[†] Satya Prathyusha Bhamidimarri,^{||} Jejoong Yoo,[‡] Bertalan Gyenes,[†] Alexander Ohmann,[†] Mathias Winterhalter,^{||} Aleksei Aksimentiev,^{*,‡} and Ulrich F. Keyser^{*,†}

[†]Cavendish Laboratory, University of Cambridge, Cambridge CB3 0HE, United Kingdom

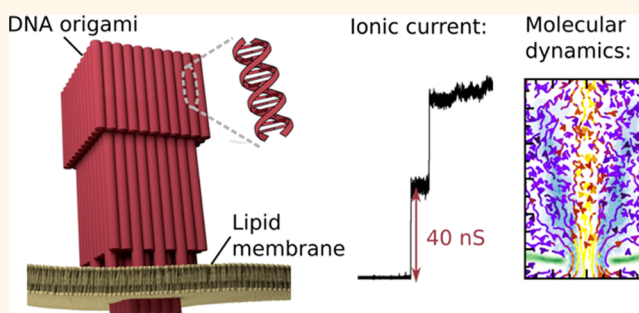
[‡]Center for the Physics of Living Cells, Department of Physics, University of Illinois at Urbana–Champaign, 1110 West Green Street, Urbana, Illinois 61801, United States

^{||}Jacobs University Bremen, 28759 Bremen, Germany

Supporting Information

ABSTRACT: DNA nanotechnology allows for the creation of three-dimensional structures at nanometer scale. Here, we use DNA to build the largest synthetic pore in a lipid membrane to date, approaching the dimensions of the nuclear pore complex and increasing the pore-area and the conductance 10-fold compared to previous man-made channels. In our design, 19 cholesterol tags anchor a megadalton funnel-shaped DNA origami porin in a lipid bilayer membrane. Confocal imaging and ionic current recordings reveal spontaneous insertion of the DNA porin into the lipid membrane, creating a transmembrane pore of tens of nanosiemens conductance. All-atom molecular dynamics simulations characterize the conductance mechanism at the atomic level and independently confirm the DNA porins' large ionic conductance.

KEYWORDS: DNA origami, lipid membrane, synthetic porin, ionic current recordings, molecular dynamics



Due to their diverse architectures, protein channels in natural lipid membranes are capable of fulfilling a variety of functions in living cells, from the recognition of substrates to the selective transport of ions or large biomolecules between cellular compartments.¹ Synthetic channels have been proposed as components of drug-delivery systems, as antimicrobial agents, biosensors, filters, photosystems, catalysts,² or as tools for synthetic biology;³ all undoubtedly requiring tailored architectures with a high level of customizability. Efforts to create synthetic channels started three decades ago with the first account by Tabushi *et al.*⁴ and are still ongoing.⁵ The architectural variability of biological membrane proteins, spanning 1 order of magnitude in channel diameter and 3 orders of magnitude in molecular weight and conductance, remains however widely unexplored and often inaccessible due to limitations of chemical synthesis methods especially for large synthetic channels.² DNA has previously been used as an alternative highly stable and readily available chemical block for building transmembrane pores,^{6–11} but the pore's architectures have so far been limited to the following three pore types: a bundle of six DNA duplexes with a nominal inner channel diameter of 2 nm,^{6–9,11} a bundle of four duplexes with a 0.8 nm channel,¹⁰ and a single membrane-spanning

duplex which induces DNA-lipid channels at its circumference.¹² Reported conductances of these DNA channels range from 0.1¹² to 1.6 nS.^{9,11}

Here we expand the design space of synthetic lipid membrane pores beyond these limits by creating a significantly larger funnel-shaped porin from DNA origami.¹³ Made exclusively using off-the-shelf components, our DNA origami porin overcomes limitations of traditional chemical synthesis that finds creation of large channels challenging.² The nominal cross section of the DNA porin is 6 nm, Figure 1B, which is wider than the cross section of large natural porins¹⁴ and comparable to the electrical diameter of the nuclear pore complex.¹⁵ Previously, funnel-shaped large-diameter DNA origami nanopores were inserted into SiN apertures,¹⁶ however insertion of large-diameter nanopores into lipid membranes has not been described until now.

Received: June 7, 2016

Accepted: August 9, 2016

Published: August 9, 2016

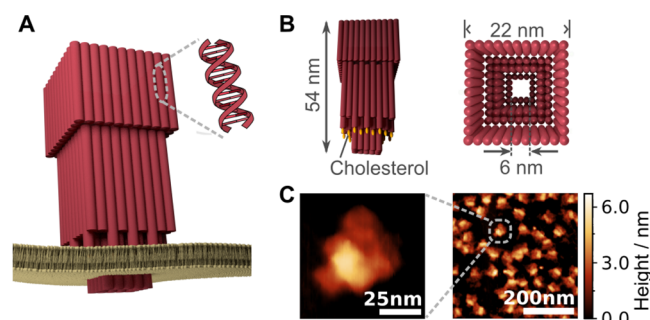


Figure 1. Design, shape, and dimensions of the DNA origami porin. (A) Envisioned positioning of the funnel-shaped DNA porin (red) in the lipid membrane (yellow), roughly drawn to scale. Each DNA duplex is represented as a red rod. (B) Design (side and top views) and dimensions of the DNA porin with 19 cholesterol tags (orange). (C) AFM images confirming the correct assembly of the DNA origami porin. Since the structures were absorbed onto mica and imaged in air, the hollow funnel with its double-layered middle section is collapsed.

RESULTS AND DISCUSSION

Design and Characterization of the DNA Origami Porin. The design of our DNA origami porin derives from that of the very first DNA nanopore,¹⁶ which has been modified to accommodate 19 cholesterol anchors to facilitate insertion into a lipid membrane. The 5 MDa DNA origami porin was assembled using the 7249 base-long M13mp18 scaffold and 179 single-stranded DNA staples. For the DNA origami layout, positions of cholesterol anchors, and DNA sequences see [Supporting Information](#), Figures S1–S4 and Tables S1–S6. Agarose gel electrophoresis yields a sharp band and confirms the stability of the structure in the measurement buffer ([Supporting Information](#), Figure S5). Atomic force microscopy (AFM) measurements, [Figure 1C](#), clearly resolve the funnel shape of the DNA origami nanopore, including its three segments with an average length of 20.8 ± 2.5 , 23.6 ± 2.1 , and 11.0 ± 1.7 nm ($n = 10$) for the wide, the middle, and the narrow sections of the porin structure, respectively, resulting in a total measured length of 55.4 nm. These values are in good agreement with the designed dimensions (20, 24, 10 nm; total length: 54 nm). For a detailed description of the image analysis see [Supporting Information](#), Note S1, Figures S6, S7, and Tables S7, S8. Assuming geometrical packing and a 2 nm diameter of the DNA helix,¹⁷ the designed square segments have a width and height of 22×22 , 18×18 , and 10×10 nm². The measured dimensions ($46.7 \pm 2.0 \times 2.67$, $35.8 \pm 2.0 \times 5.95$, and $18.9 \pm 2.0 \times 2.67$ nm²) show the collapse of the hollow funnel when imaged in air. Consequently, the middle segment of the funnel (which is made of two layers of DNA) is roughly twice as high as the other segments (which are made from a single DNA layer).

Confocal Fluorescent Imaging of Membrane Attachment. To probe effective attachment of the DNA origami porin to lipid membranes, we carried out confocal fluorescent imaging experiments. For this purpose, three Cy3-labeled fluorescent DNA oligomers were incorporated during assembly of the funnel-shaped DNA porin at its wider end. The same construct was prepared without the cholesterol membrane anchors as a negative control. After addition to giant unilamellar vesicles (GUVs), bright rings appeared around the vesicles in the confocal plane for the cholesterol-tagged

sample, [Figure 2A](#), whereas no membrane adhesion was observed for the control sample, [Figure 2B](#).

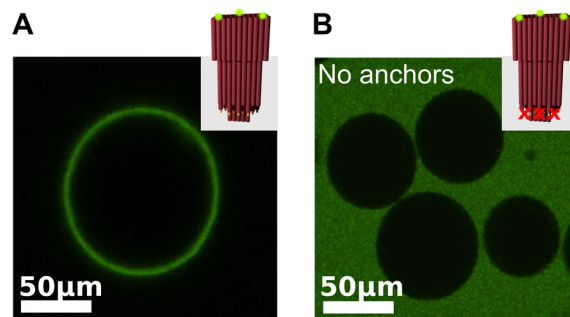


Figure 2. Fluorescent confocal images (excitation wavelength: 514 nm) of DphPC lipid vesicles after addition of the Cy3-labeled DNA origami porin, $c = 1$ nM, with (A) 19 cholesterol tags and (B) no hydrophobic tags (negative control).

Ionic Current Recordings. We subsequently carried out ionic current recordings in solvent-containing membranes¹⁸ to prove the membrane-insertion capabilities of the synthetic DNA porin and to determine its ionic conductance. As shown in [Figure 3A](#), multiple high-conductance insertion steps were

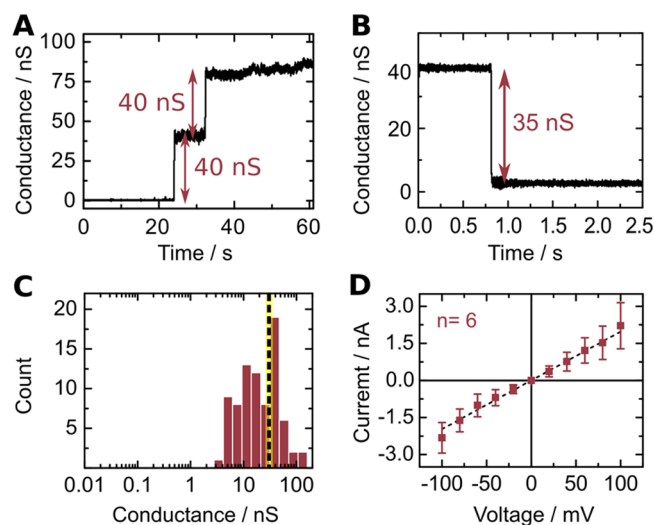


Figure 3. Ionic current recordings of the DNA origami porin in 1 M KCl, 10 mM MES, pH 6.0. (A) Exemplary current traces showing two consecutive insertions, recorded at 10 mV, and (B) a closure step, recorded at 20 mV. (C) Histogram of conductance steps with logarithmic binning including stable insertions and closures as well as insertion attempts. The dashed line at 30 nS represents the mean of the histogram. (D) Current–voltage characteristics of stable insertions of the DNA porin. Error bars correspond to the standard deviation of six independent recordings. The dashed line represents a linear fit.

observed. A stepwise decrease in conductance, [Figure 3B](#), could be caused by DNA porins escaping from the membrane. Additional insertion and closure traces are presented in the [Supporting Information](#), Figures S8 and S9. The log-scale histogram obtained from such conductance steps, [Figure 3C](#), is rather broad. The mean stepwise current increase associated with a DNA porin insertion lies at 30 nS in 1 M KCl, 10 mM 2-(*N*-morpholino)ethanesulfonic acid (MES), pH 6.0. The widespread of conductance values is likely to be caused by

multiple factors. Previous MD simulations have suggested that the conductance of DNA pores can be influenced by membrane pressure.¹⁹ Hence, a certain amount of variability is expected among experiments which involve breaking and reforming the membrane. Agarose gel electrophoresis (Supporting Information, Figure S5) indicates the presence of dimerized DNA origami porins (~15%), which could account for higher conductances if they are capable of inserting jointly. Deviations from perpendicular insertion orientation with respect to the lipid bilayer plane is likely to account for further variability.

To determine the current–voltage (I – V) characteristics of the DNA porin, only insertions which were stable across the voltage range of ± 100 mV and for the duration of the I – V recording were taken into account. I – V characteristics, Figure 3D, were found to be largely ohmic between -50 and $+50$ mV. The dashed line represents a linear fit with a gradient of 20 nS for this subset of stable insertions. A corresponding trace is shown in the Supporting Information, Figure S10. Deviations from the linear behavior are often observed above ± 50 mV: The DNA origami porins can switch to lower conductance states or disappear entirely as the voltage is increased, in line with previous observations for smaller DNA-based membrane pores.^{9,10} Rarely, the conductance increases at higher voltages while the current exhibits large fluctuations. Although some insertions could be stable for tens of minutes (Supporting Information, Figures S8E, S10), transient insertions or attempts prevail in ionic current recordings (Supporting Information, Figure S9D), contributing to the width of the reported conductance histogram.

MD Simulations. To independently evaluate the ionic conductance of our synthetic DNA-based porin, we built an all-atom model including all components of the experimental system: the DNA origami porin itself, the DphPC lipid bilayer, ions, and water molecules, Figure 4A, resulting in a system of 7,963,516 atoms. In the first 48 ns of the equilibration simulation, the DNA porin was restrained to its initial coordinates, allowing the membrane and the solvent to adopt an equilibrium configuration. The restraints were gradually removed over 14.4 ns. The system was subsequently simulated in the absence of restraints for another 19.2 ns. The DNA porin structure after free equilibration simulation is shown in the Supporting Information, Figure S12. During equilibration simulations, lipid molecules rearranged around the transmembrane part of the DNA porin, forming a water-filled passage along the DNA porins' outer surface, Figure 4B. The formation of such water-filled passages has previously been reported for a transmembrane-spanning porphyrin-tagged DNA duplex.¹² The process of lipid rearrangement is shown as a time series in the Supporting Information, Figure S11. Approximately 900 water molecules, or 50 per 180° segment of each DNA duplex, surrounded the DNA porin within a 1 nm thick rectangular slab centered at the middle plane of the membrane. The interior volume of the channel was filled with solution as well. This gives rise to an effective electrical diameter of approximately 11 nm for the DNA porin, making it larger than the electrical diameter proposed for the nuclear pore complex (6 nm).¹⁵ The equilibrium ion concentration outside the DNA porin was close to the target bulk values (1.1 M KCl and 20 mM MgCl_2); the concentration of Mg^{2+} was found to vary considerably within the system, increasing to 0.6 M within the DNA porin's walls, Supporting Information, Figure S12.

To evaluate its ionic conductance, the DNA porin was simulated at +100, +30, -30 , and -100 mV transmembrane

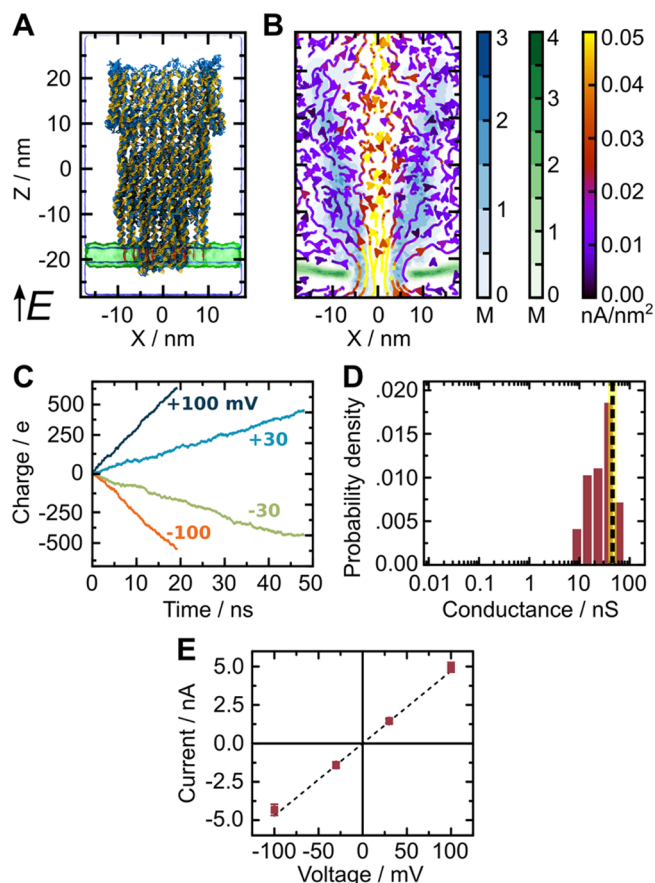


Figure 4. MD simulations of the DNA origami porin inserted into a DphPC lipid bilayer. (A) All-atom model of the DNA porin (blue and yellow) with cholesterol tags (red) embedded in a lipid membrane (green) prior to the equilibration simulation. The system contains magnesium ions in an amount sufficient to neutralize the electrical charge of the DNA porin and 1 M KCl solution (not shown). Total system size: 7,963,516 atoms. Electric field, E , in direction of positive transmembrane bias is indicated. (B) Steady-state local densities of lipid tails (carbon atoms, green color scale), DNA (phosphorus atoms, blue color scale), and ionic current (streamlines, purple-red-yellow color scale). The arrows indicate the direction of the local ionic current flux, and the color indicates the flux' magnitude. The maps were computed from a 19.2 ns long MD trajectory at a +100 mV bias sampled with a frequency of 240 ps, radially averaged about the z -axis to improve the resolution. (C) Cumulative charge transmitted across the lipid bilayer membrane at +100 mV (dark blue), +30 mV (light blue), -30 mV (green) and -100 mV (orange) transmembrane biases. The instantaneous currents were sampled every 48 ps. The cumulative charge curves were obtained by integrating the respective instantaneous current curves versus simulation time. (D) All-point conductance histograms with logarithmic binning. The conductance histograms were computed using block averaged instantaneous currents at +100, +30, -30 , and -100 mV transmembrane biases; the block average size was 2.88 ns. The dashed line indicates the mean conductance value (46.6 nS). (E) I – V characteristics. The data are block averaged with a block size of 2.88 ns. Error bars indicate the standard error of the mean, the dashed line represents a linear fit.

biases, reproducing the experimental voltage range. The duration of each MD simulation was 19.2 ns at ± 100 mV and 48 ns at ± 30 mV, which was sufficient to observe statistically significant displacement of ions within the MD trajectories.^{19–21} Supporting Information, Movie S1, described

in Note S2, illustrates the MD trajectory of the system. The cumulative charge transmitted across the lipid bilayer over time is plotted in Figure 4C. Around 80% of ions flow through the central pore, while ion flow along the outside of the channel contributes 20% to the total conductance. Figure 4D shows the histogram of the simulated conductance with a mean of 46.6 nS (dashed line, for additional conductance histograms see Supporting Information, Figure S13).

Although the width of the simulated conductance histogram is similar to that obtained from our experiments, the time scale of our MD simulation precludes us from making a definitive statement about the possible origin of broad conductance histograms. At the time scale of 50 ns, a considerable fraction of the ionic current noise is produced by thermal fluctuations.²² Another factor is the deformation of the funnel structure and fluctuations of the toroidal lipid pore, which can be appreciated from the Supporting Information, Movie S1, and snapshots of the equilibrated structure, Supporting Information, Figure S12A,B. 32% of the experimentally recorded insertion steps fall outside the conductance range obtained from MD simulations. Assuming that the simulated range is correct, this could represent the fraction of pores that inserted in an orientation different from that considered in MD simulations. In absolute numbers, 23 of the experimentally obtained insertion steps had lower conductances, potentially due to angled insertion, whereas 3 exhibited higher conductances, potentially due to the insertion of dimers. The I - V curve obtained from simulations, Figure 4E, is ohmic and yields an average conductance of 46.6 nS. The simulated conductance is thus in very good agreement with the experimental data, taking into account the difference in the access resistance conditions and systematic overestimation of bulk electrolyte conductance in the simulation.¹⁹

Coarse-Grained Simulations. To determine if the gain in free energy produced by incorporation of cholesterol anchors into a lipid bilayer membrane can indeed compensate the free energy penalty associated with the formation of a lipid pore, we estimated the free energy of pore formation using the MARTINI coarse-grained model,²³ which is known to semiquantitatively reproduce the mechanical properties of lipid bilayers.^{24,25} Starting from an equilibrated lipid bilayer system, a pore of radius R_p was created by applying a cylindrical half-harmonic wall potential to lipid molecules,²⁵ Figure 5A. Figure 5B plots the average pressure exerted by the lipid molecules on the potential wall as a function of the pore radius R_p . The pressure increases initially reaching 300 bar for $R_p = 0.5$ nm, then decreases monotonically as R_p increases, leveling off at ~ 20 bar. The work required to form a pore of radius R_p can be determined by integrating the pressure–volume (pV) work, see Methods section. Previous MD studies estimated the insertion free energy of a single cholesterol molecule into a lipid bilayer at $\Delta g_{\text{CHL}} = -75$ kJ/mol.²⁶ For the DNA porin insertion to be favorable, the sum of the pore formation work, $W_p(R_p)$, and the insertion free energy of N cholesterol anchors, $\Delta G_{\text{CHL}}(N) = N\Delta g_{\text{CHL}}$, must be negative. Figure 5C plots the value of the sum as a function of the pore radius and the number of cholesterol anchors. For the DNA porin system reported in this work, $N = 19$ and $R_p \sim 5.5$ nm (determined from the lipid headgroup density, Supporting Information, Figure S11), so $W_p(R_p) + \Delta G_{\text{CHL}}(N)$ is roughly -400 kJ/mol, a value favoring insertion of the DNA porin into a lipid bilayer.

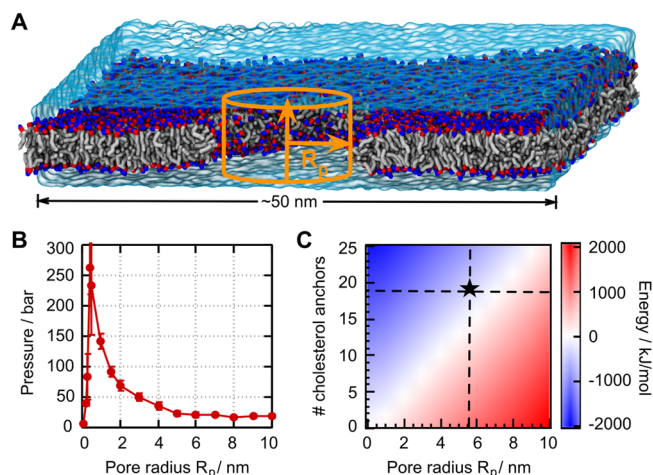


Figure 5. Simulated energetics of pore formation. (A) Setup of the coarse-grained simulation. Cut-away view of a large (50 nm on edge) patch of a lipid bilayer membrane containing a single cylindrical pore and submerged in a rectangular volume of water (blue semitransparent surface). The coarse-grained beads representing lipid hydrocarbon, phosphate, and choline are shown in gray, red, and blue, respectively. The orange cylinder indicates the half-harmonic potential wall that stabilizes the pore. (B) Pressure exerted on the half-harmonic potential wall by the lipid molecules, p_p , as a function of the pore radius, R_p . The pressure was computed by dividing the total force applied by the potential wall to the lipid molecules by the surface area, $2\pi R_p L_p$, where $L_p = 4$ nm is the lipid bilayer thickness. (C) Free energy of DNA porin insertion as a function of the pore radius and the number of cholesterol anchors. The free energy was computed as the sum of the work required to create a pore of radius R_p , $W_p(R_p)$, and the insertion free energy of N cholesterol anchors, $\Delta G_{\text{CHL}}(N)$. $W_p(R_p)$ was computed by integrating the pore formation work (pressure \times volume): $W_p(R_p) = \int_0^{R_p} p_p(r) \times 2\pi r L_p dr$. $\Delta G_{\text{CHL}}(N)$ was computed as $\Delta g_{\text{CHL}} \times N$, where the insertion free energy of a single cholesterol ($\Delta g_{\text{CHL}} = -75$ kJ/mol) was taken from a previous atomistic MD study.²⁶ The star indicates the DNA porin system described in this work.

CONCLUSION

In the present study, we have demonstrated a synthetic DNA membrane porin with the largest conductance known to date. Electrophysiological experiments and MD simulations have shown that the conductance of our DNA origami porin is over an order of magnitude larger compared to all previous DNA membrane pores. In nature, such high conductances are rare and have only been measured for few toxins^{27,28} or suggested for the nuclear pore complex. Our work demonstrates that cholesterol-based membrane anchoring is a viable method for creating larger DNA pores with diameters of several nanometers. From a methodological point of view, we introduce MD-guided design of synthetic pores by demonstrating excellent agreement between simulation and experiment.

The choice of an appropriate nanopore architecture will ultimately depend on the target application. Large scaffold-based DNA nanopores like our DNA origami porin are ideally suited for functionalization and can provide space for the passage of larger biomolecules. Such DNA pores are prime candidates for single-molecule sensing or as a research tool to study transport at molecular level if the occurrence of stable insertions can be enhanced and match the longevity of protein pores. In biological environments, our large synthetic DNA porins could mimic the behavior of toxins or more complex systems like the nuclear pore complex. With this combination

of experiments and MD simulations expanding the design space of synthetic membrane pores, we envision custom-made pores to become a versatile toolbox for cross-disciplinary applications; even if today, we may still be humble apprentices of nature.

METHODS

Design of the Cholesterol-Tagged DNA Origami Porin. The funnel-shaped DNA origami was designed on a square lattice adapted from an earlier design¹⁶ using the open source plug-in caDNAno.¹⁷ Custom DNA oligomers (for sequences see [Supporting Information](#), Tables S1–S6) were purchased from Integrated DNA Technologies, Inc.

Molecular Self-Assembly. Ten nM of the M13mp18 scaffold (New England Biolabs) was mixed with 100 nM of the 179 staples and annealed for 23 h in 40 mM Tris-HCl, 45 mM boric acid, 1 mM EDTA, 14 mM MgCl₂, pH 8.2 using a protocol described previously.²⁹

Purification. Structures were purified from excess staples *via* spin-filtration with 100 kDa MWCO filters (Amicon) in 40 mM Tris-HCl, 45 mM boric acid, 1 mM EDTA, 2 mM MgCl₂, pH 8.2. The MgCl₂ concentration was reduced to prevent sticking to the filter membrane and readjusted to 14 mM after filtration. This protocol yielded approximately 65 ng/ μ L assembled structures as determined by UV-vis spectroscopy (NanoDrop 2000, Fisher Scientific). The concentration was then adjusted to 10 nM.

Attachment of Cholesterol Anchors. The cholesterol-modified strands (3' cholesterol-TEG from Integrated DNA Technologies, 5' cholesterol-C6 from Biomers, for sequences see [Supporting Information](#), Table S6, positions are indicated in Figure S4) were heated to 50 °C for 10 min to dissolve aggregates and incubated with the DNA origami for 10 min at room temperature in 5 \times excess and 40 mM Tris-HCl, 45 mM boric acid, 1 mM EDTA, 14 mM MgCl₂ directly before each experiment.

Atomic Force Microscopy. Five μ L of the DNA origami porin (10 nM) in 10 mM Tris-HCl, 1 mM EDTA, 20 mM MgCl₂, pH 8.0 was deposited on a freshly cleaved mica surface (Agar Scientific) and incubated for 90 s. Subsequently, the surface was rinsed 3 \times with 1 mL of Milli-Q water (Merck Millipore) to remove excess sample and blow-dried with nitrogen. Imaging was carried out using a Cypher S AFM (Oxford Instruments) in amplitude modulation in air and at room temperature using AC240TS cantilevers (Olympus) with a nominal spring constant of 2 N/m. The set-point to free amplitude ratio was generally kept around 70% with a free oscillation amplitude of 20 nm. The frequency of excitation was set close to the resonance of the first flexural mode (around 70 kHz), and a repulsive mode was preferred. The scan speed was set to either 1 or 2 Hz obtaining an image of 256 \times 256 pixels. The images were flattened and band-pass filtered using Gwyddion (<http://gwyddion.net/>). Image analysis was performed as described in the [Supporting Information](#), Note S1, Figures S6, S7, and Tables S7, S8.

Lipid Vesicle Preparation. 1,2-Diphytanoyl-*sn*-glycero-3-phosphatidylcholine (DphPC; Avanti Polar Lipids), 10% cholesterol (Sigma-Aldrich) GUVs were prepared *via* electroformation using the Vesicle Prep Pro unit (Nanion technologies, Germany) and a protocol adapted from Angelova *et al.*³⁰ as previously described.¹²

Confocal Fluorescent Imaging. For confocal imaging, three staples on the wider end of the DNA origami porin were replaced by Cy3-tagged ones (Integrated DNA Technologies, see [Supporting Information](#), Figures S2, S3). Vesicles were suspended in 500 mM KCl, 10 mM MES, pH 6.0 in an incubation chamber (Grace Biolabs) and imaged using a Confocal Leica TCS SP5 microscope with a 60 \times oil immersion objective in bright field and fluorescence mode. While imaging, the fluorescently labeled DNA origami porins were added at a concentration of 1 nM, keeping the osmolarity balanced. The Cy3 tag was excited at 514 nm using an argon or a HeNe594 laser, and emission was collected above 530 nm. Images were processed using ImageJ.

Ionic Current Recordings. Ionic current recordings were carried out using solvent (*n*-decane, Alexis) containing DphPC membranes³¹ (Avanti Polar Lipids) following the detailed protocol by Gutsmann *et*

*al.*¹⁸ Solvent containing membranes are known to promote pore insertion and have previously been used for the discovery of unknown protein pores¹⁸ or DNA channels.¹² Current data were acquired at a sampling rate of 1 kHz using an Axopatch 200B amplifier and analyzed in Matlab and Clampfit. After a stable membrane was formed, the DNA porin (in 40 mM Tris-HCl, 45 mM boric acid, 1 mM EDTA, 14 mM MgCl₂, pH 8.2) was added to the *cis*-side at concentrations between 0.5 and 1.0 nM in 1 M KCl, 10 mM MES, pH 6.0. Additional ionic current recordings were carried out on the nanolipid bilayer setup³² under the same buffer conditions using a procedure described before.¹⁰

General MD Methods. All MD simulations were performed using the program NAMD2,³³ periodic boundary conditions, the CHARMM36 parameter set for water, ions, and nucleic acids,³⁴ CHARMM parameters for the DphPC lipid bilayer,³⁵ custom parametrization of ion–DNA and ion–ion interactions.³⁶ All simulations employed a 2–2–6 fs multiple timestepping, SETTLE algorithm to keep water molecules rigid,³⁷ RATTLE algorithm to keep all other covalent bonds involving hydrogen atoms rigid,³⁸ a 8–10–12 Å cutoff for van der Waals and short-range electrostatic forces. Long-range electrostatic interactions were computed using the particle mesh Ewald (PME) method³⁹ over a 1.2 Å resolution grid.⁴⁰

Assembly of the Simulation System. The caDNAno design of the DNA origami porin was converted to idealized all-atom structures using a previously described method.⁴¹ Reproducing the experimental system, cholesterol groups were added to termini of selected DNA strands; the cholesterol groups were initially placed to orient normal to the plane of the lipid bilayer. Before inserting into the lipid membrane, the DNA origami structure was simulated using the all-atom MD method for 1 ns in vacuum under a network of elastic restraints which allowed the structure to globally relax its conformation.⁴² The DphPC lipid membranes were prepared by replicating a small patch of a pre-equilibrated lipid bilayer. After merging the synthetic DNA porin with the DphPC lipid membrane, DphPC molecules located either within 3 Å of the DNA porin or inside the channel were removed. Mg²⁺-hexahydrates³⁶ were randomly placed near the DNA origami porin in the amount required to exactly compensate the electrical charge of the latter. Following that, water and 1 M KCl were added using the Solvate and Autoionize plugins of VMD.

Equilibration of the All-Atom Model. To equilibrate the DNA origami porin, we first cut away a 11 nm slab of the initial all-atom model containing the lipid membrane (5 nm thick) and the adjacent 6 nm-thick cross-section of the solvated DNA origami. The resulting system was energy-minimized for 1200 steps and equilibrated for 48 ns, allowing the lipid bilayer and the solution to adopt equilibrium conformation around the structure; the DNA atoms were restrained to maintain their initial coordinates during this equilibration simulation (with the spring constant $k_{\text{spring}} = 1 \text{ kcal}/(\text{mol } \text{Å}^2)$). Following that, the equilibrated lipid bilayer and the surrounding solvent were combined with the full-length DNA origami porin. The resulting system was equilibrated under a network of elastic restraints that maintained distances between atomic pairs at their initial values; such elastic restraints excluded hydrogen atoms, phosphate groups, atoms in the same nucleotide, and pairs separated by more than 8 Å. The system was simulated under such elastic restraints for 14.4 ns; the spring constants of the restraints were decreased from 0.5 to 0.1 and then to 0.01 kcal/(mol Å²) every 4.8 ns. All equilibration simulations were performed under the NPT condition, where the number of atoms (*N*), pressure (*P*), and temperature (*T*) were kept constant. The pressure was set to 1 atm using the Nosé–Hoover Langevin piston method.^{43,44} The temperature was maintained at 295 K using a Langevin thermostat.⁴⁵ The ratios of the system's dimensions along the *x* and *y* axis were constrained, while the *z* axis was decoupled. Following that, the system was simulated in the absence of any restraints for 19.2 ns. During all MD simulations, the system's coordinates were recorded every 48 ps.

MD Simulation of Ionic Current. All simulations of the ionic current were performed in the constant number of atom, volume, and temperature ensemble. A voltage drop, *V*, across the system was produced by applying an external electric field *E* such that $V = -EL$,

where L was the length of the simulation system in the direction of the applied field.⁴⁶

Ionic Current Calculations. Prior to calculations of the ionic current, frames of the MD trajectory were aligned⁴⁶ using a two-step process. First, we shifted the x and y coordinates of all atoms in the simulation system by the same amount to maintain the center of mass coordinate of the DNA origami porin constant within the plane of the lipid bilayer. Next, the z -coordinates of all atoms in the system were shifted by the same amount to maintain the z -coordinate of the lipid bilayer center of mass constant. To reduce thermal noise originating from stochastic displacements of ions in the bulk solution, the ionic current calculations were carried out within the $-l/2 \leq z \leq l/2$ region of the system, where $l = 30$ Å. The instantaneous current was computed as

$$I\left(t + \frac{\Delta t}{2}\right) = \frac{1}{\Delta t l} \sum_i^N q_i (\zeta_i(t + \Delta t) - \zeta_i(t)) \quad (1)$$

where

$$\zeta_i(t) = \begin{cases} z_i(t), & |z_i(t)| \leq l/2 \\ -l/2, & z_i(t) < -l/2 \\ l/2, & z_i(t) > l/2 \end{cases} \quad (2)$$

the sum over i indicates a sum over all ions, Δt is the time interval between two consecutive frames of the MD trajectory, and q_i is the charge of ion i .⁴⁷ The average current of a trajectory was computed by summing up all instantaneous currents and dividing by the number of coordinate frames of the trajectory. To estimate the error, the ionic current trace was first block averaged with a block size of 2.88 ns. The reported standard errors of the mean were calculated from the block-averaged current traces.

Calculations of the Local Density and Local Ionic Current Flux. The local density and the local ionic current flux were computed as described previously.²¹ We divided the simulation system into $5 \times 5 \times 5$ Å grids and calculated the average density of the selected atom groups and average flux of each ion species in each grid using a sampling frequency of 240 ps. The local current in each grid in a given direction (x , y , or z) was calculated by

$$I_j = \sum_i q_i \times f_{i,j}, \quad (i = \text{K}^+, \text{Cl}^-, \text{Mg}^{2+}; j = x, y, z) \quad (3)$$

where i is the ion species (K^+ , Cl^- , or Mg^{2+}), q_i is the charge of the ion, and $f_{i,j}$ is the flux of the ion in the given direction. We averaged the three-dimensional (3D) density and flux data in the cylindrical coordinate over the azimuthal angle to obtain the mean density and mean flux on the $r - z$ plane as described previously.¹⁹ Following that, the 2D density and flux were made symmetric about the z axis by making a mirror image ($r \rightarrow -r$). Finally, we used the contourf and streamplot function in the python matplotlib package to generate the local density and flux plots, which were then assembled into the final figures.

Coarse-Grained Simulation of Lipid Pore Formation. The MARTINI simulations were performed using the Gromacs 5.0.4 package with a 20 fs time step and 12 Å cutoffs for nonbonded forces.⁴⁸ The half-harmonic potential was implemented using the MDRUN program of the Gromacs package.²⁵ First, we equilibrated a lipid bilayer membrane containing 8192 dioleoyl-phosphatidylcholine (DOPC) lipid molecules and 96,000 water beads in a $50 \times 50 \times 9$ nm³ simulation box at zero surface tension under periodic boundary condition. We chose to simulate DOPC lipids over DphPC because the current MARTINI force field does not provide parametrization for DphPC. DOPC is analogous to DphPC within the MARTINI's coarse-graining framework that maps four hydrocarbon atoms to one MARTINI bead. Following that, multiple systems, each containing a single pore of prescribed radius, were created by applying a half-harmonic cylindrical potential, $V_p(r)$, to all DOPC beads: $V_p(r) = 0.5k(r - R_p)^2$ for $r < R_p$ and 0 otherwise, where R_p is the pore radius and r is the distance from the pore axis. Each system was simulated for

300 ns; the average pressure was computed using the last 200 ns of simulation. The error bars were estimated as the standard error of 10 ns block averages.

ASSOCIATED CONTENT

Supporting Information

The Supporting Information is available free of charge on the ACS Publications website at DOI: 10.1021/acsnano.6b03759.

Layout, positioning of cholesterol anchors, and DNA sequences of the DNA origami porin, agarose gel electrophoresis, analysis of AFM imaging, additional ionic current traces. Results of MD simulations including arrangement of lipid head groups at lipid–DNA interface, local concentration of ions near the DNA origami porin, histograms of the simulated ionic current, and caption describing the Movie S1 (PDF)
Movie S1 (AVI)

AUTHOR INFORMATION

Corresponding Authors

*E-mail: aksiment@illinois.edu.

*E-mail: ufk20@cam.ac.uk.

Author Contributions

[§]These authors contributed equally.

Notes

The authors declare no competing financial interest.

ACKNOWLEDGMENTS

The authors thank K. C. Gödel for help with 3D sketches and E. Hemmig for critical reading of the manuscript. K.G. acknowledges funding from the Winton Programme for the Physics of Sustainability, Gates Cambridge, and the Oppenheimer Ph.D. studentship; U.F.K. from an ERC Consolidator Grant (Designerpores 647144); and M.R. from the Early Postdoc Mobility fellowship of the Swiss National Science Foundation. A.A., J.Y., and C.Y.L. acknowledge support from the National Science Foundation under grants DMR-1507985, PHY-1430124, and EEC-1227034 and the supercomputer time provided through XSEDE Allocation grant MCA05S028 and the Blue Waters petascale supercomputer system (UIUC). M.W. and S.P.B. acknowledge support from Marie Skłodowska Curie Actions within the Initial Training Networks Translocation Network, project no. 607694.

REFERENCES

- (1) Alberts, B.; Johnson, A.; Lewis, J.; Raff, M.; Roberts, K.; Walter, P. *Molecular Biology of the Cell*; Garland Science: New York, 2002.
- (2) Sakai, N.; Matile, S. Synthetic Ion Channels. *Langmuir* **2013**, *29*, 9031–9040.
- (3) Czogalla, A.; Franquelim, H. G.; Schwille, P. DNA Nanostructures on Membranes as Tools for Synthetic Biology. *Biophys. J.* **2016**, *110*, 1698–1707.
- (4) Tabushi, I.; Kuroda, Y.; Yokota, K. A,B,D,F-Tetrasubstituted β -Cyclodextrin as Artificial Channel Compound. *Tetrahedron Lett.* **1982**, *23*, 4601–4604.
- (5) Mamad-Hemouch, H.; Ramoul, H.; Abou Taha, M.; Bacri, L.; Huin, C.; Przybylski, C.; Oukhaled, A.; Thiebot, B.; Patriarche, G.; Jarroux, N.; Pelta, J. Biomimetic Nanotubes Based on Cyclodextrins for Ion-Channel Applications. *Nano Lett.* **2015**, *15*, 7748–7754.
- (6) Langecker, M.; Arnaut, V.; Martin, T. G.; List, J.; Renner, S.; Mayer, M.; Dietz, H.; Simmel, F. C. Synthetic Lipid Membrane Channels Formed by Designed DNA Nanostructures. *Science* **2012**, *338*, 932–6.

- (7) Burns, J. R.; Stulz, E.; Howorka, S. Self-Assembled DNA Nanopores That Span Lipid Bilayers. *Nano Lett.* **2013**, *13*, 2351–2356.
- (8) Burns, J. R.; Göpflich, K.; Wood, J. W.; Thacker, V. V.; Stulz, E.; Keyser, U. F.; Howorka, S. Lipid-Bilayer-Spanning DNA Nanopores with a Bifunctional Porphyrin Anchor. *Angew. Chem., Int. Ed.* **2013**, *52*, 12069–72.
- (9) Seifert, A.; Göpflich, K.; Burns, J. R.; Fertig, N.; Keyser, U. F.; Howorka, S. Bilayer-Spanning DNA Nanopores with Voltage-Switching between Open and Closed State. *ACS Nano* **2015**, *9*, 1117–1126.
- (10) Göpflich, K.; Zettl, T.; Meijering, A. E. C.; Hernández-Ainsa, S.; Kocabey, S.; Liedl, T.; Keyser, U. F. DNA-Tile Structures Lead to Ionic Currents through Lipid Membranes. *Nano Lett.* **2015**, *15*, 3134–3138.
- (11) Burns, J. R.; Seifert, A.; Fertig, N.; Howorka, S. A Biomimetic DNA-Based Channel for the Ligand-Controlled Transport of Charged Molecular Cargo Across a Biological Membrane. *Nanotechnol.* **2016**, *11*, 152–156.
- (12) Göpflich, K.; Li, C.-Y.; Mames, I.; Bhamidimarri, S. P.; Ricci, M.; Yoo, J.; Mames, A.; Ohmann, A.; Winterhalter, M.; Stulz, E.; Aksimentiev, A.; Keyser, U. F. Ion Channels Made from a Single Membrane-Spanning DNA Duplex. *Nano Lett.* **2016**, *16*, 4665–4669.
- (13) Rothmund, P. W. K. Folding DNA to Create Nanoscale Shapes and Patterns. *Nature* **2006**, *440*, 297–302.
- (14) Benz, R. Biophysical Properties of Porin Pores from Mitochondrial Outer Membrane of Eukaryotic Cells. *Experientia* **1990**, *46*, 131–137.
- (15) Mazzanti, M.; Bustamante, J. O.; Oberleithner, H. Electrical Dimension of the Nuclear Envelope. *Physiol. Rev.* **2001**, *81*, 1–19.
- (16) Bell, N. A. W.; Engst, C. R.; Ablay, M.; Divitini, G.; Ducati, C.; Liedl, T.; Keyser, U. F. DNA Origami Nanopores. *Nano Lett.* **2012**, *12*, 512–517.
- (17) Douglas, S. M.; Marblestone, A. H.; Teerapittayanon, S.; Vazquez, A.; Church, G. M.; Shih, W. M. Rapid Prototyping of 3D DNA-Origami Shapes with CaDNano. *Nucleic Acids Res.* **2009**, *37*, 5001–6.
- (18) Gutschmann, T.; Heimburg, T.; Keyser, U.; Mahendran, K. R.; Winterhalter, M. Protein Reconstitution into Freestanding Planar Lipid Membranes for Electrophysiological Characterization. *Nat. Protoc.* **2015**, *10*, 188–198.
- (19) Yoo, J.; Aksimentiev, A. Molecular Dynamics of Membrane-Spanning DNA Channels: Conductance Mechanism, Electro-Osmotic Transport, and Mechanical Gating. *J. Phys. Chem. Lett.* **2015**, *6*, 4680–4687.
- (20) Aksimentiev, A. Deciphering Ionic Current Signatures of DNA Transport through a Nanopore. *Nanoscale* **2010**, *2*, 468–483.
- (21) Li, C.-Y.; Hemmig, E. A.; Kong, J.; Yoo, J.; Keyser, U. F.; Aksimentiev, A. Ionic Conductivity, Structural Deformation and Programmable Anisotropy of DNA Origami in Electric Field. *ACS Nano* **2015**, *9*, 1420–1433.
- (22) Bhattacharya, S.; Yoo, J.; Aksimentiev, A. Water Mediates Recognition of DNA Sequence via Ionic Current Blockade in a Biological Nanopore. *ACS Nano* **2016**, *10*, 4644–4651.
- (23) Monticelli, L.; Kandasamy, S.; Periolo, X.; Larson, R.; Tieleman, D. P.; Marrink, S. J. The MARTINI Coarse Grained Force Field: Extension to Proteins. *J. Chem. Theory Comput.* **2008**, *4*, 819–834.
- (24) Ollila, O. H. S.; Risselada, H. J.; Louhivuori, M.; Lindahl, E.; Vattulainen, I.; Marrink, S. J. 3D Pressure Field in Lipid Membranes and Membrane-Protein Complexes. *Phys. Rev. Lett.* **2009**, *102*, 078101.
- (25) Yoo, J.; Jackson, M. B.; Cui, Q. A Comparison of Coarse-Grained and Continuum Models for Membrane Bending in Lipid Bilayer Fusion Pores. *Biophys. J.* **2013**, *104*, 841–852.
- (26) Bennett, W. F. D.; Tieleman, D. P. Molecular Simulation of Rapid Translocation of Cholesterol, Diacylglycerol, and Ceramide in Model Raft and Nonraft Membranes. *J. Lipid Res.* **2012**, *53*, 421–429.
- (27) Haug, T. M.; Sand, S. L.; Sand, O.; Phung, D.; Granum, P. E.; Hardy, S. P. Formation of Very Large Conductance Channels by *Bacillus Cereus* Nhe in Vero and GH(4) Cells Identifies NheA + B as the Inherent Pore-Forming Structure. *J. Membr. Biol.* **2010**, *237*, 1–11.
- (28) Meera, P.; Wallner, M.; Toro, L. A Neuronal Beta Subunit (KCNMB4) Makes the Large Conductance, Voltage- and Ca²⁺-Activated K⁺ Channel Resistant to Charybdotoxin and Iberitoxin. *Proc. Natl. Acad. Sci. U. S. A.* **2000**, *97*, 5562–7.
- (29) Hernández-Ainsa, S.; Bell, N. A. W.; Thacker, V. V.; Göpflich, K.; Misiunas, K.; Fuentes-Perez, M. E.; Moreno-Herrero, F.; Keyser, U. F. DNA Origami Nanopores for Controlling DNA Translocation. *ACS Nano* **2013**, *7*, 6024–30.
- (30) Angelova, M. I.; Dimitrov, D. S. Liposome Electroformation. *Faraday Discuss. Chem. Soc.* **1986**, *81*, 303.
- (31) Mueller, P.; Rudin, D. O.; Tien, H. T.; Wescott, W. C. Reconstitution of Cell Membrane Structure in Vitro and its Transformation into an Excitable System. *Nature* **1962**, *194*, 979–980.
- (32) Göpflich, K.; Kulkarni, C. V.; Pambos, O. J.; Keyser, U. F. Lipid Nanobilayers to Host Biological Nanopores for DNA Translocations. *Langmuir* **2013**, *29*, 355–364.
- (33) Phillips, J. C.; Braun, R.; Wang, W.; Gumbart, J.; Tajkhorshid, E.; Villa, E.; Chipot, C.; Skeel, R. D.; Kale, L.; Schulten, K. Scalable Molecular Dynamics with NAMD. *J. Comput. Chem.* **2005**, *26*, 1781–1802.
- (34) MacKerell, A. D., Jr.; Bashford, D.; Bellott, M.; Dunbrack, R. L., Jr.; Evanseck, J.; Field, M. J.; Fischer, S.; Gao, J.; Guo, H.; Ha, S.; Joseph, D.; Kuchnir, L.; Kuczera, K.; Lau, F. T. K.; Mattos, C.; Michnick, S.; Ngo, T.; Nguyen, D. T.; Prodhom, B.; Reiher, I. W. E.; et al. All-Atom Empirical Potential for Molecular Modeling and Dynamics Studies of Proteins. *J. Phys. Chem. B* **1998**, *102*, 3586–3616.
- (35) Lim, J. B.; Klauda, J. B. Lipid Chain Branching at the Iso- and Anteiso-Positions in Complex Chlamydia Membranes: A Molecular Dynamics Study. *Biochim. Biophys. Acta, Biomembr.* **2011**, *1808*, 323–31.
- (36) Yoo, J.; Aksimentiev, A. Improved Parametrization of Li⁺, Na⁺, K⁺, and Mg²⁺ Ions for All-Atom Molecular Dynamics Simulations of Nucleic Acid Systems. *J. Phys. Chem. Lett.* **2012**, *3*, 45–50.
- (37) Miyamoto, S.; Kollman, P. A. SETTLE: An Analytical Version of the SHAKE and RATTLE Algorithm for Rigid Water Molecules. *J. Comput. Chem.* **1992**, *13*, 952–962.
- (38) Andersen, H. C. RATTLE: A “Velocity” Version of the SHAKE Algorithm for Molecular Dynamics Calculations. *J. Comput. Phys.* **1983**, *52*, 24–34.
- (39) Batcho, P. F.; Case, D. A.; Schlick, T. Optimized Particle-Mesh Ewald/Multiple-Time Step Integration for Molecular Dynamics Simulations. *J. Chem. Phys.* **2001**, *115*, 4003–4018.
- (40) Skeel, R. D.; Hardy, D. J.; Phillips, J. C. Correcting Mesh-Based Force Calculations to Conserve Both Energy and Momentum in Molecular Dynamics Simulations. *J. Comput. Phys.* **2007**, *225*, 1–5.
- (41) Yoo, J.; Aksimentiev, A. In Situ Structure and Dynamics of DNA Origami Determined through Molecular Dynamics Simulations. *Proc. Natl. Acad. Sci. U. S. A.* **2013**, *110*, 20099–20104.
- (42) Maffeo, C.; Yoo, J.; Aksimentiev, A. De Novo Reconstruction of DNA Origami Structures through Atomistic Molecular Dynamics Simulation. *Nucleic Acids Res.* **2016**, *44*, 3013–3019.
- (43) Martyna, G. J.; Tobias, D. J.; Klein, M. L. Constant Pressure Molecular Dynamics Algorithms. *J. Chem. Phys.* **1994**, *101*, 4177–4189.
- (44) Feller, S. E.; Zhang, Y. H.; Pastor, R. W.; Brooks, B. R. Constant Pressure Molecular Dynamics Simulation – the Langevin Piston Method. *J. Chem. Phys.* **1995**, *103*, 4613–4621.
- (45) Brünger, A. T. *X-PLOR, Version 3.1: A System for X-ray Crystallography and NMR*; The Howard Hughes Medical Institute and Department of Molecular Biophysics and Biochemistry, Yale University: New Haven, CT, 1992.
- (46) Aksimentiev, A.; Schulten, K. Imaging α -Hemolysin with Molecular Dynamics: Ionic Conductance, Osmotic Permeability and the Electrostatic Potential Map. *Biophys. J.* **2005**, *88*, 3745–3761.
- (47) Aksimentiev, A.; Heng, J. B.; Timp, G.; Schulten, K. Microscopic Kinetics of DNA Translocation through Synthetic Nanopores. *Biophys. J.* **2004**, *87*, 2086–2097.

(48) Hess, B.; Kutzner, C.; van der Spoel, D.; Lindahl, E. GROMACS 4: Algorithms for Highly Efficient, Load-Balanced, and Scalable Molecular Simulation. *J. Chem. Theory Comput.* **2008**, *4*, 435–447.